

# DRKF: Distilled Rotated Kernel Fusion for Efficient Rotation Invariant Descriptors in Local Feature Matching

Ranran Huang<sup>1</sup>, Jiancheng Cai<sup>1</sup>, Chao Li<sup>2</sup>, Zhuoyuan Wu<sup>1</sup>, Xinmin Liu<sup>1</sup>, Zhenhua Chai<sup>1</sup>

**Abstract**—The performance of local feature descriptors degrades in the presence of large rotation variations. To address this issue, we present an efficient approach to learning rotation invariant descriptors. Specifically, we propose Rotated Kernel Fusion (RKF) which imposes rotations on the convolution kernel to improve the inherent nature of CNN. Since RKF can be processed by the subsequent re-parameterization, no extra computational costs will be introduced in the inference stage. Moreover, we present Multi-oriented Feature Aggregation (MOFA) which aggregates features extracted from multiple rotated versions of the input image and can provide auxiliary knowledge for the training of RKF by leveraging the distillation strategy. We refer to the distilled RKF model as DRKF. Besides the evaluation on a rotation-augmented version of the public dataset HPatches, we also contribute a new dataset named DiverseBEV which is collected during the drone’s flight and consists of bird’s eye view images with large viewpoint changes and camera rotations. Extensive experiments show that our method can outperform other state-of-the-art techniques when exposed to large rotation variations.

## I. INTRODUCTION

Local feature matching between images is essential for multiple computer vision tasks, including Structure from Motion (SfM) [1] and Simultaneous Localization and Mapping (SLAM) [2]. In recent years, this field has obtained significant development due to the advance in deep learning, however, it is still challenging to find reliable corresponding points across images with large geometric transformations and appearance differences caused by camera rotations.

Traditional local descriptors including SIFT [3], SURF [4] and ORB [5] employ a detector-descriptor pipeline and explicitly assign orientations to each keypoint, thereby achieving rotation invariance by design. Recently, numerous learning-based methods have proved their potential in dealing with complicated cases. Methods like LIFT [6], LF-Net [7], and RF-Net [8] follow the idea of SIFT [3] and predict the shape parameters based on which image patches around each keypoint are cropped and warped for further description. However, the process brings huge computational costs and fails to handle very large rotation changes due to the lack of explicit labels. On the contrary, most popular learning-based implementations like SuperPoint [9], D2-Net [10], R2D2 [11] and ASLFeat [12] directly locate the keypoints

and compute their descriptors using CNN without considering orientations, therefore there exists a more significant performance gap in the presence of large rotation variations. Although there are some methods aiming to obtain rotation invariant features [13], [14], [15], [16], [17], they increase the computational overhead and the difficulty with deployment in embedded devices.

In this paper, we address the challenge of large or even extreme rotation changes by making the following contributions to improve rotation invariance efficiently:

- Shown in Fig. 1 and Fig. 2, we propose Rotated Kernel Fusion (RKF) to impose rotations on each convolution kernel followed by fusion on features extracted by multiple rotated filters. Employing RKF, we enable CNN to be rotation invariant inherently. Eventually, we leverage re-parameterization to make the computational cost remain the same in the inference stage without affecting the performance.
- By introducing multiple rotation transformations to the input images and conducting feature ensemble, we introduce Multi-oriented Feature Aggregation (MOFA) shown in Fig. 1, which is further used as a teacher in the knowledge distillation pipeline to supervise the model equipped with RKF operation.
- Due to the lack of publicly available aerial-view datasets with large viewpoint changes and camera rotations, we construct a new dataset named DiverseBEV which is collected during the drone’s flight.
- Our experimental results show that DRKF improves rotation invariance considerably and outperforms other state-of-the-art approaches remarkably on rotation-augmented HPatches [18] and the new DiverseBEV dataset without introducing extra computational cost in the inference phase.

## II. RELATED WORKS

### A. Local Feature Matching

Hand-crafted methods including SIFT [3], SURF [4] and ORB [5] have dominated the field for a long time. Many classical descriptors compute the orientations of detected keypoints, so that they can be rotation invariant by design. For example, SIFT [3] first selects the keypoints using local extrema detection in the pyramid of Difference of Gaussian (DoG) and obtains orientations with the Histogram of Oriented Gradients (HOG). Some other methods obtain the orientation based on intensity. For instance, ORB [5] first detects keypoints with FAST [19] in different scales and then

<sup>1</sup>Ranran Huang, Jiancheng Cai, Zhuoyuan Wu, Xinmin Liu and Zhenhua Chai are with Meituan, No.7 Rongda Road, Chaoyang District, Beijing, 100012, China {huangranran, caijiancheng, wuzhuoyuan02, liuxinmin, chaizhenhua}@meituan.com

<sup>2</sup>Chao Li is with School of Artificial Intelligence, Beijing University of Posts and Telecommunications, No.10 Xitucheng Road, Haidian District, Beijing, 100876, China chaoli@bupt.edu.cn

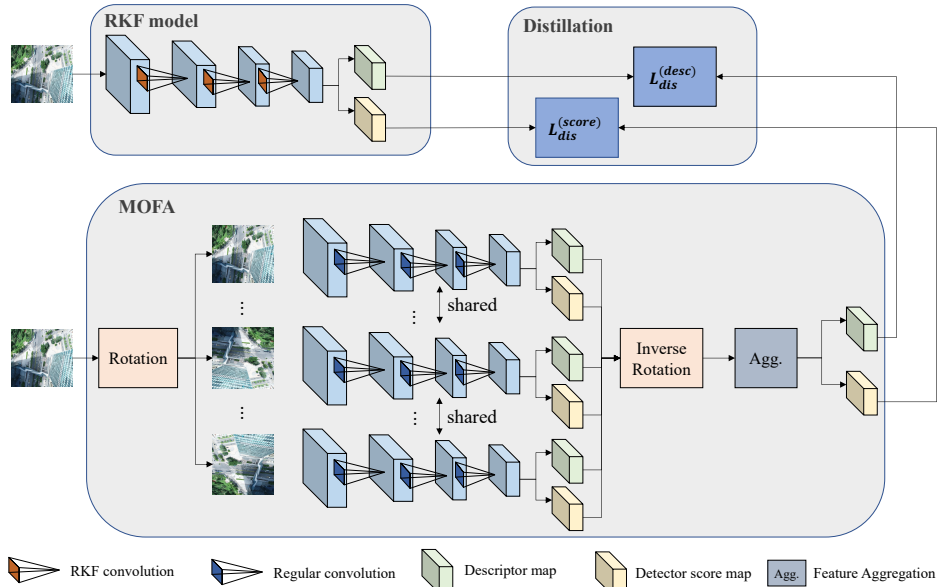


Fig. 1. The figure shows the framework of our method. We follow the detection-and-description framework to jointly optimize the detection and description objectives. The RKF model replaces the regular convolution with RKF convolution and improves the inherent nature of CNN (see details in Fig. 2). MOFA integrates the features extracted from multiple rotated versions of images and serves as the teacher model to provide auxiliary supervision to the RKF model. The distillation stage generates the distilled RKF model (DRKF).

takes the direction from the corner’s center to the intensity centroid in a local window as the orientation. Despite the robustness to rotation, they lack the ability to cope with complex cases caused by weak or repeated textures and illumination changes.

Recently, we see major improvements in learning-based methods which offer promising advances in the capability of dealing with complicated cases. In terms of rotation invariance, methods including LIFT [6], LF-Net [7], RF-Net [8] imitate the traditional methods and predict the orientation and scale parameters. The pipeline usually consists of feature detection, patch sampling with spatial transform network (STN) [20] and feature description. However, it is challenging to regress feature scales and orientations accurately without explicit labels. In addition, patch sampling and warping for numerous detected keypoints are computationally expensive. On the contrary, recent techniques like SuperPoint [9], D2-Net [10] and ASLFeat [12] achieve state-of-the-art results. For example, D2-Net and ASLFeat use a detect-and-describe approach, and couple the capability of the feature detector and descriptor by deriving keypoints from the same feature maps that are used for extracting feature descriptors. However, they neglect the orientations of keypoints, therefore fail to demonstrate steady performance when exposed to extreme viewpoint variations. The same problem still exists for recent local feature matching techniques like SuperGlue [21] and LoFTR [22].

To obtain transformation invariant descriptors, GIFT [17] uses group convolutions [13] to exploit underlying structures of the extracted features from the transformed versions of an image. RoRD [16] is based on D2-Net [10] and achieves rotation-robustness by training with in-plane rotated images and performing correspondence ensemble, however, its expressive capacity is still limited by the inherent nature

of CNN. There are some other CNN-based alternatives developed for rotation-equivariance [13], [14], [23], [15], [24], however, they require to re-design the CNN architectures, leading to increasing computational burden in the inference stage or difficulty with deployment in embedded devices. Compared to these methods, our method 1) improves the inherent property of convolution layers without altering the architecture for inference; 2) aggregates the features extracted from rotated versions of input images just for auxiliary supervision in the training phase, which introduces no extra computational overhead for inference.

### B. Re-parameterization

Generally, models with multi-branch aggregation usually demonstrate stronger learning ability [25], [26] despite being more computationally expensive. Re-parameterization is a significant technique that has been frequently used for better performance while reducing computational costs in the inference stage. Some successful implementations like RepLKNet [27], RepVGG [26] and ACNet [28] show that re-parameterization can be adopted to integrate the multiple branches equivalently and improve inference efficiency.

For our proposed RKF model, a multi-branch structure is applied within each convolution layer. By virtue of the re-parameterization approach, the model can be equally slimmed to the original single-branch structure, thus reducing the computation cost considerably.

### C. Knowledge Distillation (KD)

Knowledge Distillation (KD) aims to supervise a light student model with a cumbersome teacher model and can be adopted for model compression. KD is considered to be an effective method in multiple tasks, including classification [29], [30], [31], object detection [32], [33] and semantic segmentation [34], [35]. In this paper, we propose to leverage the

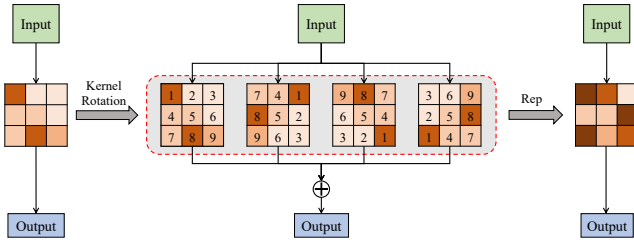


Fig. 2. The structure of RKF convolution in the case of  $3 \times 3$  kernel. RKF imposes kernel rotation on the original kernel, and fuses features extracted by multi-oriented kernels. Re-parameterization can be further leveraged to convert the multiple kernels to one single kernel.

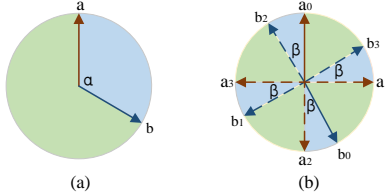


Fig. 3. Visualized explanation of MOFA in the case of four rotation transformations on the input pair of images. (a) The two original corresponding keypoints  $a$  and  $b$  with an orientation gap of  $\alpha$ . (b) The transformed corresponding keypoints on two images under four rotation transformations. The orientations of  $a$  and  $b$  are transformed to  $a_0, a_1, a_2, a_3$  and  $b_0, b_1, b_2, b_3$ , respectively, generating multiple correspondence pairs with an orientation gap of  $\beta$ . Instead of matching the two original keypoints with an orientation gap of  $\alpha$  on two images, the model only needs to consider several correspondence pairs with a smaller gap of  $\beta$  on the transformed keypoints.

distillation strategy for auxiliary knowledge when training our proposed RKF model.

### III. METHODS

In this section, we describe each component of our method, i.e. Rotated Kernel Fusion (RKF) and Multi-oriented Feature Aggregation (MOFA). We make the most of MOFA by applying it as a teacher to supervise the RKF model in a manner of knowledge distillation.

#### A. Feature correspondences

a) *General loss for detection-and-description:* We follow most existing detection-and-description approaches like D2-Net [10] and ASLFeat [12], and adopt the loss function as Eq.1 to jointly optimize the detection and description objectives:

$$\mathcal{L}_{ori} = \frac{1}{C} \sum_{c \in C} \frac{s_c s'_c}{\sum_{q \in C} s_q s'_q} \mathcal{M}(f_c, f'_c), \quad (1)$$

where  $C$  is the ground-truth correspondence set,  $s_c$  and  $s'_c$  are corresponding scores,  $f_c$  and  $f'_c$  refer to corresponding descriptors, and  $\mathcal{M}(\cdot, \cdot)$  is the ranking loss for representation learning, which can be defined as triplet [36] or contrastive loss [37].

b) *Homography Augmentation:* Similar to [16], we incorporate in-plane rotations in augmentations on the training data to simulate realistic viewpoint changes. Given an image pair, we augment either image of the pair using a random homography transformation consisting of  $0-2\pi$  rotations. This increases the data diversity and enables the model to be exposed to extreme rotations in the training stage. Besides the

in-plane rotations, we also incorporate scaling, skewness and perspectivity transformations in the augmentations as done in [9].

#### B. Rotated Kernel Fusion (RKF)

a) *Equivariance properties of CNNs:* Let  $\mathbf{M}_1 \in \mathbb{R}^{N \times C_1 \times H_1 \times W_1}$ ,  $\mathbf{M}_2 \in \mathbb{R}^{N \times C_2 \times H_2 \times W_2}$  be the input and output feature map, respectively. We use  $*$  as the convolution operator, and  $\mathbf{W} \in \mathbb{R}^{C_2 \times C_1 \times k \times k}$  to denote the kernel of a  $k \times k$  convolution kernel with  $C_1$  input channels and  $C_2$  output channels. Therefore the regular convolution can be denoted as  $\mathbf{M}_2 = \mathbf{M}_1 * \mathbf{W}$ . Convolution layers can be used effectively in a deep network because all the layers are translation equivariant: shifting the input and then feeding it through the convolution layer is the same as feeding the original input through the same layer and then shifting the result, which can be represented as follows:

$$[L_t \mathbf{M}_1] * \mathbf{W} = L_t[\mathbf{M}_1 * \mathbf{W}], \quad (2)$$

where  $L_t$  denotes the translation transformation.

However, CNNs are not rotation invariant inherently, which means rotating the input and then convolving it with a filter is not the same as first convolving and then rotating the result. In fact, the convolution of a rotated input  $L_r \mathbf{M}_1$  with a filter  $\mathbf{W}$  is equal to the rotation of the result obtained by original input  $\mathbf{M}_1$  convolving with the inverse-rotated filter  $L_r^{-1} \mathbf{W}$  [13]. This can be formulated as:

$$[L_r \mathbf{M}_1] * \mathbf{W} = L_r[\mathbf{M}_1 * L_r^{-1} \mathbf{W}], \quad (3)$$

where  $L_r$  denotes the rotation transformation.

b) *Motivation and Design:* Because CNNs are not rotation invariant inherently, they are susceptible to large rotation changes. To improve the inherent nature of convolution layers, inspired by Group equivariant CNN (G-CNN) [13], we propose Rotated Kernel Fusion (RKF) which imposes rotations on each convolution kernel and fuses the feature maps extracted by multi-oriented kernels, shown in Fig. 2. The major difference from [13] is that we choose summation instead of concatenation for the fusion of the multi-oriented feature maps. Using summation operation, multiple kernels can be merged into one single kernel with the original shape by the subsequent re-parameterization operation to obtain higher efficiency and convenience in deployment.

We split the rotation range into  $N-1$  intervals and denote the rotation transformation on each kernel  $\mathbf{W}$  as  $L_r^{\theta_n}$  where  $\theta_n = \frac{2\pi}{N}n$ ,  $0 \leq n \leq N-1$  refers to the angle of rotation.

$$L_r^{\theta_n} = \begin{bmatrix} \cos(\theta_n) & -\sin(\theta_n) \\ \sin(\theta_n) & \cos(\theta_n) \end{bmatrix} \quad (4)$$

This transformation matrix acts on points in  $\mathbb{Z}^2$  (pixel coordinates) by multiplying the matrix  $L_r^{\theta_n}$  by the coordinate vector  $x(u, v)$  of a point:

$$L_r^{\theta_n} x = \begin{bmatrix} \cos(\theta_n) & -\sin(\theta_n) \\ \sin(\theta_n) & \cos(\theta_n) \end{bmatrix} \begin{bmatrix} u \\ v \end{bmatrix} \quad (5)$$

The RKF convolution is denoted as:

$$\mathbf{M}_2 = \mathbf{M}_1 * \mathbf{W}_{RKF} = \sum_{n=0}^{N-1} (\mathbf{M}_1 * [L_r^{\theta_n} \mathbf{W}]), \theta_n = \frac{2\pi}{N}n. \quad (6)$$

To validate the equivariance of RKF, we suppose the RKF convolution layer is fed with a rotated image or feature map  $L_r^{\theta_m} \mathbf{M}_1$ ,  $0 \leq m \leq N-1$ , then the result is:

$$[L_r^{\theta_m} \mathbf{M}_1] * \mathbf{W}_{RKF} = \sum_{n=0}^{N-1} ([L_r^{\theta_m} \mathbf{M}_1] * [L_r^{\theta_n} \mathbf{W}]). \quad (7)$$

Based on Eq. 3, we let  $\mathbf{W} = L_r \mathbf{W}$  and obtain:

$$[L_r \mathbf{M}_1] * [L_r \mathbf{W}] = L_r [\mathbf{M}_1 * \mathbf{W}]. \quad (8)$$

Then based on Eq. 8 and the property that rotation by  $\theta_{-m}$  is the same as the rotation by  $\theta_{N-m}$ , we can rewrite Eq. 7 as:

$$\begin{aligned} [L_r^{\theta_m} \mathbf{M}_1] * \mathbf{W}_{RKF} &= L_r^{\theta_m} \sum_{n=0}^{N-1} (\mathbf{M}_1 * [L_r^{\theta_{N-m-n}} \mathbf{W}]) \\ &= L_r^{\theta_m} \sum_{n=-m}^{N-1-m} (\mathbf{M}_1 * [L_r^{\theta_n} \mathbf{W}]) \\ &= L_r^{\theta_m} \sum_{n=0}^{N-1} (\mathbf{M}_1 * [L_r^{\theta_n} \mathbf{W}]) \\ &= L_r^{\theta_m} [\mathbf{M}_1 * \mathbf{W}_{RKF}]. \end{aligned} \quad (9)$$

Therefore, RKF enables the convolution to be equivariant to rotation, which means rotating the input and then feeding it through the layers is the same as feeding the original input and then rotating the result. Accordingly, the local feature descriptors can obtain better invariance to rotation: the local descriptors are the same for two corresponding points on a pair of images with relative rotation. Although the above conclusions are based on discrete rotation angles, in fact, for an image rotated by a randomly sampled angle, the orientation difference between the rotated image and the nearest rotated filter is limited to at most  $\frac{\pi}{N}$ , enhancing the robustness of rotations.

We call the ordinary model with regular convolution layers **base model**, and the new model with RKF convolution layers **RKF model** in the following sections.

*c) Re-parameterization:* Because those operations introduced by RKF are linear within each convolution layer, we can further use re-parameterization to fuse multiple trained kernels into a single one for inference. In this way, RKF will not alter the original CNN architecture and introduce extra computation in the inference phase. According to Eq. 6, we can obtain the final single kernel  $\mathbf{W}_{RKF} \in \mathbb{R}^{C_2 \times C_1 \times k \times k}$  as follows:

$$\mathbf{W}_{RKF} = \sum_{n=0}^{N-1} (L_r^{\theta_n} \mathbf{W}) \quad (10)$$

### C. Distilled Rotated Kernel Fusion (DRKF)

*a) Multi-oriented Feature Aggregation (MOFA):* While RKF leads to significant performance gains in local feature matching under extreme rotation variations, we observe that the training optimization is faced with several drawbacks: 1) Different rotated kernels share the same parameters of the original filter, therefore imbalanced training might be caused when the contribution of some rotated kernels overweight others; 2) For the purpose of re-parameterization, no non-linear operations are involved before the integration of the results from different rotated kernels. To overcome these limitations, we propose another structure called Multi-oriented Feature Aggregation (**MOFA**) to provide auxiliary supervision for RKF. MOFA conducts post-processing on the base model trained with homography augmentations. Formally, we use  $F_{base}(\cdot)$  to represent the base model that projects the input to the descriptor or detector score map and use  $F_{MOFA}(\cdot)$  to denote the projection of MOFA. The input image  $\mathbf{I}$  is rotated by  $N$  different angles respectively, and then fed into the trained base model to get the corresponding outputs, which are further aggregated as follows:

$$F_{MOFA}(\mathbf{I}) = \frac{1}{N} \sum_{n=0}^{N-1} L_r^{-\theta_n} (F_{base}(L_r^{\theta_n}(\mathbf{I}))), \theta_n = \frac{2\pi}{N}n. \quad (11)$$

Therefore each rotated branch of MOFA incorporates non-linearity and contributes independently and equally, which compensates for the limitations of RKF training. We can understand MOFA intuitively in Fig. 3: multiple rotation transformations convert the original large orientation gap of two corresponding points on the input pair of images to a smaller gap, which generates features that are more robust to large rotation variations.

*b) Knowledge Distillation:* For MOFA, the increase in rotation invariance comes at a cost of multiple feedforwards, making it computationally expensive for embedded devices. On the other hand, the training optimization of computationally efficient RKF is affected by the tangled branches of rotated kernels and the lack of non-linear activation before feature fusion. Therefore, we propose to utilize a knowledge distillation strategy and take advantage of MOFA to provide auxiliary supervision to the RKF model. Suppose the normalized dense descriptor map and detector score map generated by the MOFA is  $D^{(t)} \in \frac{H}{r} \times \frac{W}{r} \times C$  and  $S^{(t)} \in H \times W \times 1$  respectively, and those generated by the RKF are denoted as  $D^{(s)} \in \frac{H}{r} \times \frac{W}{r} \times C$  and  $S^{(s)} \in H \times W \times 1$  respectively, where  $H$  and  $W$  refer to height and width of the input image respectively, and  $r$  is the downsampling rate. The distillation loss of descriptors is defined in the form of mean distance error, which is formulated as:

$$\mathcal{L}_{dis}^{(desc)} = \frac{r^2}{HW} \sum_{i,j} \left\| D_{ij}^{(s)} - D_{ij}^{(t)} \right\|_2. \quad (12)$$

And the distillation loss of the score map is in the form of local cross-entropy loss. We reshape the two score maps  $S^{(s)}$  and  $S^{(t)}$  to  $\frac{H}{r} \times \frac{W}{r} \times r^2$  with inverse pixel shuffle [38]

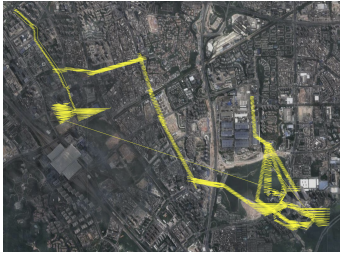


Fig. 4. The flight trajectory of the DiverseBEV dataset.

operation, and define the distillation loss of the score map as:

$$\mathcal{L}_{dis}^{(score)} = -\frac{r^2}{HW} \sum_{i,j} \sum_{k=1}^{r^2} P_{ijk}^{(t)} \log P_{ijk}^{(s)}, \quad (13)$$

where

$$P_{ijk} = \exp(S_{ijk}) / \sum_k \exp(S_{ijk}). \quad (14)$$

The total distillation loss is a combination of Eq. 12 and Eq. 13, which is

$$\mathcal{L}_{dis} = \mathcal{L}_{dis}^{(desc)} + \lambda_1 \mathcal{L}_{dis}^{(score)}. \quad (15)$$

Therefore, the total training loss of our method is formulated as:

$$\mathcal{L} = \mathcal{L}_{ori} + \lambda_2 \mathcal{L}_{dis}. \quad (16)$$

In this way, we obtain the distilled RKF model, which is referred to as **DRKF model**. Similarly, we can also obtain the distilled base model by transferring knowledge from MOFA to the base model, which is called **DBase model** in our following sections.

#### IV. EXPERIMENTS

##### A. Datasets

a) *GL3D* [39]: This dataset is only used for training. It contains 181,280 high-resolution images in 1073 different scenes, along with the image matches, the intrinsics, and extrinsics, as well as the depth data.

b) *HPatches* [18]: Out of the 116 available sequences, we selected 108 as implemented in [10] for evaluation. Each sequence consists of 6 images of illumination changes (52 sequences) or viewpoint changes (56 sequences). The original dataset is called Standard HPatches in our experiments. Besides, we also use the Rotated HPatches dataset constructed by [16] which is the augmented version of the original dataset with random in-plane rotation of images from 0 to  $2\pi$ .

c) *DiverseBEV*: Currently, most existing works for local feature matching are based on ground-view datasets [18], [16], [10], [12]. Compared to the ground-view cameras, the aerial-view platforms, e.g., drones, capture the scene image from the sky with a wider angle, less occlusion and more comprehensive viewpoints, therefore the aerial-view data can be useful to investigate the rotation invariance of local descriptors. Due to the lack of publicly available aerial-view datasets with high viewpoint changes and camera rotations, we introduce a new dataset called DiverseBEV. This dataset comprises bird’s eye view outdoor scenarios captured during

the drone’s flight, thus exhibiting large or even extreme rotation variations. First, 5292 images at a resolution of  $5472 \times 3648$  are collected using an FC6310R camera on DJI M300 aircraft with an average altitude of 207m in Shenzhen, China. We take RTK as a priori, implement 3D reconstruction with COLMAP [1], [40] with GPS Position Prior<sup>1</sup>, and obtain  $K$ ,  $R$ ,  $T$  and depth for each image which is taken as ground truth intrinsic, extrinsic parameters, and depth information. We traverse all images and select all image pairs with a distance from 20m to 50m according to the  $T$  of each image. Then, based on the rotation angle  $R$  of each image, the relative rotation angle of each pair of images is obtained. For relative rotation angles ranging from  $0^\circ$  to  $360^\circ$ , around 25 image pairs are randomly sampled every  $10^\circ$  for evaluation, thus 901 image pairs are sampled in total which constitute our DiverseBEV dataset. For this dataset, evaluation is done using the model trained only on GL3D, therefore demonstrating the generalizability of our proposed method. For a depiction of the flight path see Fig. 4.

##### B. Experimental Settings

In the training phase, we first train the base model with homography augmentations for 400,000 iterations with a learning rate of 0.1. The trained base model is used to construct MOFA. Then the RKF model is trained with 100,000 iterations with the supervision of MOFA. We set  $n = 4$  in Eq. 6 and Eq. 11, therefore the rotation angles in MOFA and RKF are  $0, \pi/2, \pi, 3\pi/2$ . For loss hyperparameters, we set  $\lambda_1 = \lambda_2 = 1$  in Eq. 15 and Eq. 16.

##### C. Evaluation Protocol

a) *Mean Matching Accuracy (MMA)*: We follow the standard protocol [10] for evaluating nearest neighbor feature matching on HPatches dataset. For each image pair of HPatches, we match the descriptors extracted by each method using nearest neighbor search with the mutual test. A match is considered to be correct if the back-projection of the keypoint estimated by the ground truth homography matrix falls within a given pixel threshold. We vary the threshold and record the mean matching accuracy (MMA) [41] over all pairs, which is the average percentage of correct matches per image pair<sup>2</sup>.

b) *Mean Average Accuracy (MAA)*: For DiverseBEV, we follow [42] and we compute the angular difference, in degrees, between the estimated and ground-truth quaternion vectors of two cameras. Distance difference is computed between the estimated and ground-truth translation vectors. We then threshold the differences over varying values for all possible pairs of images, which renders a curve. We compute the Mean Average Accuracy (MAA) by integrating this curve up to a maximum threshold ( $10^\circ$  and 10m for the angular and distance error respectively)<sup>3</sup>.

<sup>1</sup><https://github.com/Vincentqyw/colmap-gps>

<sup>2</sup>Evaluation code: <https://github.com/mihaidusmanu/d2-net>

<sup>3</sup>Evaluation code: <https://www.kaggle.com/competitions/image-matching-challenge-2022>

TABLE I

EVALUATION RESULTS FOR MMA ON THE HPATCHES DATASET USING PIXEL THRESHOLDS 6/8/10.

Methods	Rotation Aug	Standard	Rotated	Average
SIFT [3]	–	0.52/0.54/0.54	0.51/0.51/0.52	0.54/0.53/0.53
SuperPoint [9]	✓	0.69/0.71/0.73	0.21/0.22/0.22	0.45/0.46/0.48
D2-Net [10]	✗	0.73/0.81/0.84	0.17/0.20/0.22	0.45/0.50/0.53
ASLFeat [12]	✗	0.81/0.82/0.82	0.22/0.24/0.24	0.52/0.53/0.53
GIFT [17]	✓	0.83/0.86/0.87	0.43/0.44/0.44	0.63/0.65/0.66
RoRD [16]	✓	0.79/0.84/0.86	0.48/0.59/0.64	0.64/0.72/0.75
(Ours) DRKF*	✓	<b>0.84/0.86/0.87</b>	<b>0.80/0.81/0.82</b>	<b>0.82/0.84/0.85</b>

\* Same results for DRKF after re-parameterization.

#### D. Comparison with SOTA approaches

In this part, we first compare our proposed method with SIFT [3] and existing state-of-the-art learning-based approaches. It is notable that DRKF after re-parameterization shares the same results as DRKF in TABLE I and II.

a) *HPatches*: Different methods are compared on Standard HPatches, Rotated HPatches, and the average of two in TABLE I, in terms of the mean matching accuracy (MMA) of all pairs over pixel thresholds 6, 8, and 10. This setting for thresholds is the same as implemented in [16]. The "Rotation Aug" column denotes whether the rotation augmentation is adopted during the training process. For SIFT [3], SuperPoint [9], D2-Net [10] and RoRD [16], we directly quote the statistics reported in [16]. To validate the performance of ASLFeat [12] and GIFT [17] we use the trained model provided by the original authors. In this part, we mainly focus on feature extraction, therefore we do not compare our approach to SOTA feature matching approaches, e.g. SuperGlue [21] and LoFTR [22]. According to the results, it can be observed that the performance of SuperPoint [9], D2-Net [10] and ASLFeat [12] degrades greatly on rotation-augmented datasets, while SIFT shows steady performance under random rotation due to its elaborate design for orientation prediction. GIFT [17] and RoRD [16] are trained with homography augmentations and are specifically designed to improve rotation invariance, therefore they overtake other methods on Rotated Hpatches. However, our DRKF still surpasses them by a large margin, for example, 32% better than RoRD with regards to MMA over a threshold of 6 on Rotated Hpatches. It is notable that the proposed DRKF even outperforms SIFT considerably when testing on the rotation-augmented dataset while retaining the performance on standard datasets. This demonstrates that DRKF effectively enables the network to extract more rotation-invariant features.

b) *DiverseBEV*: We resize images of the DiverseBEV dataset to  $600 \times 1000$  and compare DRKF to other SOTA methods for Mean Average Accuracy (MAA) curves on the DiverseBEV dataset, shown in Fig. 5. For SIFT, we use its OpenCV implementation. For learning-based methods, we use the trained model provided by the original authors. In this part, we also involve state-of-the-art feature matching methods like SuperGlue [21] and LoFTR [22]. It can be seen that our DRKF obtains the largest MAA over varying angular or distance thresholds. TABLE II shows the integration result of these curves up to  $10^\circ$  or/and 10m. The third

TABLE II

EVALUATION RESULTS FOR MAA ON THE DIVERSEBEV DATASET. THE NUMBERS ARE OBTAINED BY INTEGRATING THE CORRESPONDING CURVES IN FIG. 5.

Methods	Rotation Aug	MAA ( $10^\circ$ &10m)	MAA ( $10^\circ$ )	MAA (10m)
SIFT [3]	–	0.3096	0.5741	0.3103
SuperPoint [9]+SuperGlue [21]	✓	0.1388	0.2574	0.1428
D2-Net [10]	✗	0.0319	0.0807	0.0331
ASLFeat [12]	✗	0.0789	0.1548	0.0809
LoFTR [22]	✗	0.0583	0.1226	0.0592
GIFT [17]	✓	0.1200	0.2410	0.1216
RoRD [16]	✓	0.1833	0.5110	0.1848
(Ours) DRKF*	✓	<b>0.3914</b>	<b>0.7523</b>	<b>0.3966</b>

\* Same results for DRKF after re-parameterization.

TABLE III

INFERENCE TIME ON NVIDIA TX2

Methods	Inference Time (ms)
SuperPoint [9] + SuperGlue [21]	110
RoRD [16]	229
ASLFeat [12]	56
MOFA	207
Base	58
DRKF	213
DRKF (*Rep)	57

\*Rep refers to re-parameterization.

column shows the integration of MAA over both angular and distance thresholds. The last two columns are with regard to angular threshold up to  $10^\circ$  and distance threshold up to 10m, respectively. It can be seen from the third column that SIFT overtakes all previous learning-based methods, while our method obtains 8.18% performance gain over SIFT on average MAA. Since the DiverseBEV dataset displays large rotation variations of the camera during the drone's flight, the experiments can show that although our method is based on in-plane rotation operations, it also works for real-world out-of-plane rotations and can perform stably under extreme viewpoint changes.

#### E. Ablation Studies

To analyze the effectiveness of each component of our DRKF, we conduct ablation experiments on Standard Hpatches and Rotated Hpatches respectively. There are 5 variants considered in our experiments: the base model, RKF model, MOFA, DBase and DRKF model, which are all introduced in Section III. All experiments are implemented with homography augmentation of training data. The results are shown in Fig. 7, from which it can be concluded that:

- For Standard Hpatches, different methods show similar results, while DRKF still achieves the best matching performance under varying thresholds.
- The performance of the base model degrades severely on Rotated Hpatches, on the contrary, the matching performance of RKF is more steady.
- MOFA explicitly integrates multi-oriented features of the base model, therefore outperforms the base model on rotation-augmented datasets remarkably.
- With the supervision of MOFA, DBase overtakes the base model significantly, while still lagging behind

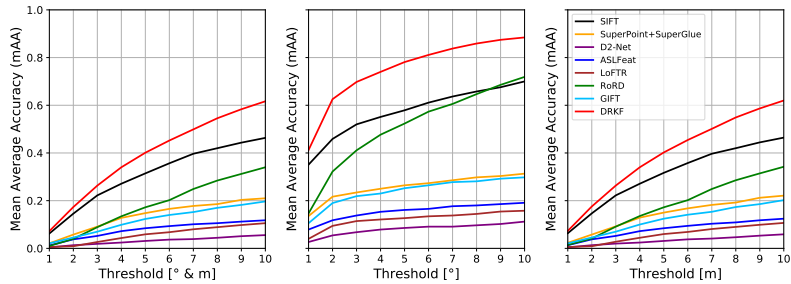


Fig. 5. Mean average accuracy (MAA) curves on the DiverseBEV dataset. The left shows the MAA of image pairs satisfying both angular and distance thresholds. The middle and right are the MAA as a function of the angular threshold and distance threshold, respectively. Our DRKF outperforms other SOTA methods on the DiverseBEV dataset.

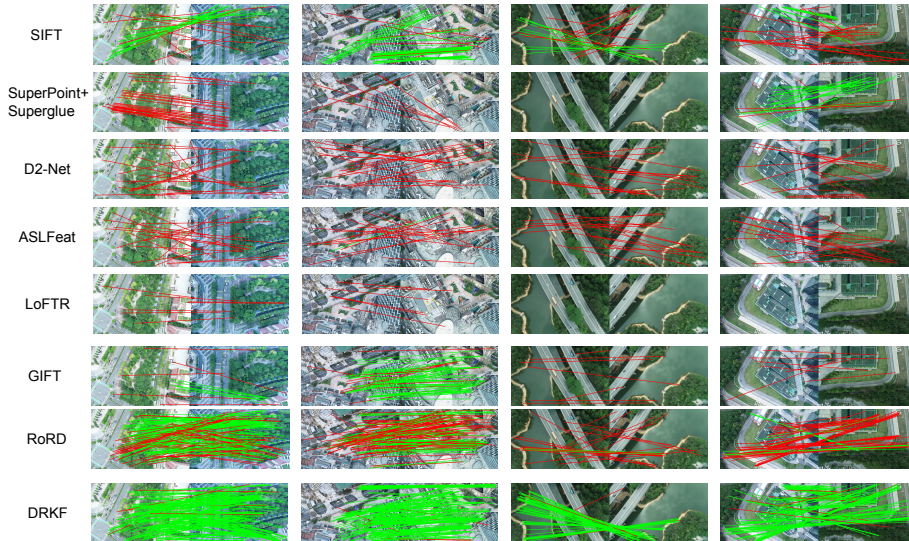


Fig. 6. Qualitative results on the DiverseBEV Dataset. Our method DRKF (bottom) outperforms all other methods by a significant margin. These correspondences are filtered by RANSAC-based geometric verification to obtain a final set of feature correspondences. A match is considered to be correct if the backprojection of the keypoint estimated using the ground truth  $K$ ,  $R$ ,  $T$  and depth falls within a pixel threshold of 1.5. We use red lines for wrong matches, and green for correct matches.

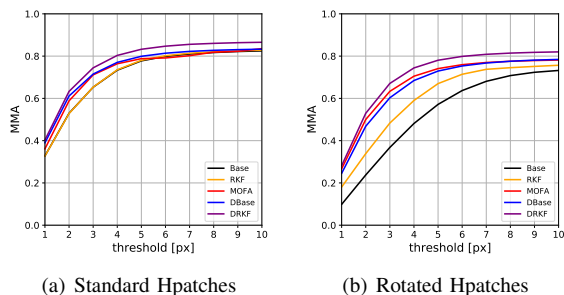


Fig. 7. Ablation studies on Standard HPatches and Rotated HPatches image pairs. For each variant, the mean matching accuracy (MMA) as a function of the pixel threshold is shown. DRKF achieves the best overall performance on Rotated HPatches.

DRKF because of the inherent nature of CNN. DRKF utilizes rotated kernels to enhance the representation ability for rotation invariance, therefore surpasses any other variants, including its teacher, MOFA.

To summarize, two components of DRKF, i.e. RKF and its teacher MOFA, all contribute to rotation invariance.

#### F. Qualitative comparison

Qualitative comparison can provide an intuitive observation of the matching results of different methods. We

compare our DRKF with SIFT and learning-based methods, including SuperPoint [9] + SuperGlue [21], D2-Net [10], ASLFeat [12], LoFTR [22], GIFT [17], and RoRD [16] in Fig. 6. We can see that compared to other methods, DRKF obtains the largest number of correct correspondences under different rotation variations, which shows that it can generalize effectively under large viewpoint changes, and even outperforms SIFT which explicitly assigns orientation to each keypoint.

#### G. Efficiency Analysis

For efficiency analysis, we compare the inference time of each method on Nvidia TX2 at the input size of  $640 \times 360$  in TABLE III. It can be seen that MOFA consumes longer inference time than the base model due to multi-feedforward feature aggregation. By virtue of the reparameterization technique, DRKF can be accelerated, and become computationally comparable to the base model.

### V. CONCLUSION

In this paper, we present an effective framework for creating rotation-invariant descriptors to find correspondences under challenging viewpoint conditions. The key part of our method is RKF, which imposes rotations on each convolution

kernel. Thanks to the re-parameterization technique, the rotated kernels can be further merged into one single kernel with the original shape so that the computational cost remains the same. We further propose MOFA to provide auxiliary supervision for RKF. Experiments indicate that our method can improve the rotation invariance of feature descriptors remarkably on both HPatches and the DiverseBEV dataset.

## REFERENCES

- [1] J. L. Schonberger and J.-M. Frahm, "Structure-from-motion revisited," in *Proc. IEEE Conf. Comput. Vis. Pattern Recognit. (CVPR)*, pp. 4104–4113, 2016.
- [2] R. Mur-Artal, J. M. M. Montiel, and J. D. Tardos, "Orb-slam: a versatile and accurate monocular slam system," *IEEE Trans. Robot.*, vol. 31, no. 5, pp. 1147–1163, 2015.
- [3] D. G. Lowe, "Distinctive image features from scale-invariant keypoints," *Int. J. Comput. Vis. (IJCV)*, vol. 60, no. 2, pp. 91–110, 2004.
- [4] H. Bay, A. Ess, T. Tuytelaars, and L. Van Gool, "Speeded-up robust features (surf)," *Comput. Vis. Image. Und.*, vol. 110, no. 3, pp. 346–359, 2008.
- [5] E. Rublee, V. Rabaud, K. Konolige, and G. Bradski, "Orb: An efficient alternative to sift or surf," in *Proc. IEEE Int. Conf. Comput. Vision. (ICCV)*, pp. 2564–2571, Ieee, 2011.
- [6] K. M. Yi, E. Trulls, V. Lepetit, and P. Fua, "Lift: Learned invariant feature transform," in *Proc. Eur. Conf. Comput. Vis. (ECCV)*, pp. 467–483, Springer, 2016.
- [7] Y. Ono, E. Trulls, P. Fua, and K. M. Yi, "Lf-net: Learning local features from images," in *Proc. Adv. Neural Inf. Process. Syst. (NeurIPS)*, vol. 31, 2018.
- [8] X. Shen, C. Wang, X. Li, Z. Yu, J. Li, C. Wen, M. Cheng, and Z. He, "RF-net: An end-to-end image matching network based on receptive field," in *Proc. Eur. Conf. Comput. Vis. (ECCV)*, pp. 8132–8140, 2019.
- [9] D. DeTone, T. Malisiewicz, and A. Rabinovich, "Superpoint: Self-supervised interest point detection and description," in *Proc. IEEE Int. Conf. Comput. Vision. (ICCV) Workshop*, pp. 224–236, 2018.
- [10] M. Dusmanu, I. Rocco, T. Pajdla, M. Pollefeys, J. Sivic, A. Torii, and T. Sattler, "D2-net: A trainable cnn for joint description and detection of local features," in *Proc. IEEE Conf. Comput. Vis. Pattern Recognit. (CVPR)*, pp. 8092–8101, 2019.
- [11] J. Revaud, C. De Souza, M. Humenberger, and P. Weinzaepfel, "R2d2: Reliable and repeatable detector and descriptor," in *Proc. Adv. Neural Inf. Process. Syst. (NeurIPS)*, vol. 32, 2019.
- [12] Z. Luo, L. Zhou, X. Bai, H. Chen, J. Zhang, Y. Yao, S. Li, T. Fang, and L. Quan, "Aslfeat: Learning local features of accurate shape and localization," in *Proc. IEEE Conf. Comput. Vis. Pattern Recognit. (CVPR)*, pp. 6589–6598, 2020.
- [13] T. Cohen and M. Welling, "Group equivariant convolutional networks," in *International conference on machine learning*, pp. 2990–2999, PMLR, 2016.
- [14] T. S. Cohen and M. Welling, "Steerable cnns," *arXiv preprint arXiv:1612.08498*, 2016.
- [15] G. Bökman and F. Kahl, "A case for using rotation invariant features in state of the art feature matchers," in *Proceedings of the IEEE/CVF Conference on Computer Vision and Pattern Recognition*, pp. 5110–5119, 2022.
- [16] U. S. Parihar, A. Gujarathi, K. Mehta, S. Tourani, S. Garg, M. Milford, and K. M. Krishna, "Rord: Rotation-robust descriptors and orthographic views for local feature matching," in *2021 IEEE/RSJ International Conference on Intelligent Robots and Systems (IROS)*, pp. 1593–1600, IEEE, 2021.
- [17] Y. Liu, Z. Shen, Z. Lin, S. Peng, H. Bao, and X. Zhou, "Gift: Learning transformation-invariant dense visual descriptors via group cnns," *Advances in Neural Information Processing Systems*, vol. 32, 2019.
- [18] V. Balntas, K. Lenc, A. Vedaldi, and K. Mikolajczyk, "Hpatches: A benchmark and evaluation of handcrafted and learned local descriptors," in *Proc. IEEE Conf. Comput. Vis. Pattern Recognit. (CVPR)*, pp. 5173–5182, 2017.
- [19] E. Rosten and T. Drummond, "Machine learning for high-speed corner detection," in *Proc. Eur. Conf. Comput. Vis. (ECCV)*, pp. 430–443, Springer, 2006.
- [20] M. Jaderberg, K. Simonyan, A. Zisserman, et al., "Spatial transformer networks," in *Proc. Adv. Neural Inf. Process. Syst. (NeurIPS)*, vol. 28, 2015.
- [21] P.-E. Sarlin, D. DeTone, T. Malisiewicz, and A. Rabinovich, "Super-glue: Learning feature matching with graph neural networks," in *Proc. IEEE Conf. Comput. Vis. Pattern Recognit. (CVPR)*, pp. 4938–4947, 2020.
- [22] J. Sun, Z. Shen, Y. Wang, H. Bao, and X. Zhou, "Loftr: Detector-free local feature matching with transformers," in *Proc. IEEE Conf. Comput. Vis. Pattern Recognit. (CVPR)*, pp. 8922–8931, 2021.
- [23] M. Weiler and G. Cesa, "General e (2)-equivariant steerable cnns," *Advances in Neural Information Processing Systems*, vol. 32, 2019.
- [24] A. Peri, K. Mehta, A. Mishra, M. Milford, S. Garg, and K. M. Krishna, "Ref-rotation equivariant features for local feature matching," *arXiv preprint arXiv:2203.05206*, 2022.
- [25] C. Szegedy, W. Liu, Y. Jia, P. Sermanet, S. Reed, D. Anguelov, D. Erhan, V. Vanhoucke, and A. Rabinovich, "Going deeper with convolutions," in *Proc. IEEE Conf. Comput. Vis. Pattern Recognit. (CVPR)*, pp. 1–9, 2015.
- [26] X. Ding, X. Zhang, N. Ma, J. Han, G. Ding, and J. Sun, "Repyvgg: Making vgg-style convnets great again," in *Proc. IEEE Conf. Comput. Vis. Pattern Recognit. (CVPR)*, pp. 13733–13742, 2021.
- [27] X. Ding, X. Zhang, J. Han, and G. Ding, "Scaling up your kernels to 31x31: Revisiting large kernel design in cnns," in *Proc. IEEE Conf. Comput. Vis. Pattern Recognit. (CVPR)*, pp. 11963–11975, 2022.
- [28] X. Ding, Y. Guo, G. Ding, and J. Han, "Acnet: Strengthening the kernel skeletons for powerful cnn via asymmetric convolution blocks," in *Proc. IEEE Int. Conf. Comput. Vision. (ICCV)*, pp. 1911–1920, 2019.
- [29] G. Hinton, O. Vinyals, J. Dean, et al., "Distilling the knowledge in a neural network," in *Proc. Adv. Neural Inf. Process. Syst. (NeurIPS) Workshop*, 2014.
- [30] Z. Li and D. Hoiem, "Learning without forgetting," *IEEE Trans. Pattern Anal. Mach. Intell. (TPAMI)*, vol. 40, no. 12, pp. 2935–2947, 2017.
- [31] Z. Peng, Z. Li, J. Zhang, Y. Li, G.-J. Qi, and J. Tang, "Few-shot image recognition with knowledge transfer," in *Proc. IEEE Int. Conf. Comput. Vision. (ICCV)*, pp. 441–449, 2019.
- [32] G. Chen, W. Choi, X. Yu, T. Han, and M. Chandraker, "Learning efficient object detection models with knowledge distillation," in *Proc. Adv. Neural Inf. Process. Syst. (NeurIPS)*, vol. 30, 2017.
- [33] Q. Li, S. Jin, and J. Yan, "Mimicking very efficient network for object detection," in *Proc. IEEE Conf. Comput. Vis. Pattern Recognit. (CVPR)*, pp. 6356–6364, 2017.
- [34] T. He, C. Shen, Z. Tian, D. Gong, C. Sun, and Y. Yan, "Knowledge adaptation for efficient semantic segmentation," in *Proc. IEEE Conf. Comput. Vis. Pattern Recognit. (CVPR)*, pp. 578–587, 2019.
- [35] Q. Dou, Q. Liu, P. A. Heng, and B. Glocker, "Unpaired multi-modal segmentation via knowledge distillation," *IEEE Trans. Pattern Anal. Mach. Intell. (TPAMI)*, vol. 39, no. 7, pp. 2415–2425, 2020.
- [36] F. Schroff, D. Kalenichenko, and J. Philbin, "Facenet: A unified embedding for face recognition and clustering," in *Proc. IEEE Conf. Comput. Vis. Pattern Recognit. (CVPR)*, 2015.
- [37] R. Hadsell, S. Chopra, and Y. Lecun, "Dimensionality reduction by learning an invariant mapping," in *Proc. IEEE Conf. Comput. Vis. Pattern Recognit. (CVPR)*, 2006.
- [38] W. Shi, J. Caballero, F. Huszar, J. Totz, and Z. Wang, "Real-time single image and video super-resolution using an efficient sub-pixel convolutional neural network," in *Proc. IEEE Conf. Comput. Vis. Pattern Recognit. (CVPR)*, 2016.
- [39] T. Shen, Z. Luo, L. Zhou, R. Zhang, S. Zhu, T. Fang, and L. Quan, "Matchable image retrieval by learning from surface reconstruction," in *Proc. Asian Conf. Comput. Vis. (ACCV)*, 2018.
- [40] J. L. Schönberger, E. Zheng, J.-M. Frahm, and M. Pollefeys, "Pixel-wise view selection for unstructured multi-view stereo," in *Computer Vision—ECCV 2016: 14th European Conference, Amsterdam, The Netherlands, October 11–14, 2016, Proceedings, Part III 14*, pp. 501–518, Springer, 2016.
- [41] K. Mikolajczyk and C. Schmid, "A performance evaluation of local descriptors," *IEEE transactions on pattern analysis and machine intelligence*, vol. 27, no. 10, pp. 1615–1630, 2005.
- [42] Y. Jin, D. Mishkin, A. Mishchuk, J. Matas, P. Fua, K. M. Yi, and E. Trulls, "Image matching across wide baselines: From paper to practice," *International Journal of Computer Vision*, vol. 129, no. 2, pp. 517–547, 2021.